PHYSICAL REVIEW B **76**, 104411 (2007)

Role of exchange and correlation potential in calculating x-ray absorption spectra of half-metallic alloys: Mn and Cu *K*-edge XANES in Cu_2MnM Heusler alloys (M=Al, Sn, In)

K. Hatada[1,2,*] and J. Chaboy[1]
[1]*Instituto de Ciencia de Materiales de Aragón, CSIC-Universidad de Zaragoza, 50009 Zaragoza, Spain*
[2]*Laboratori Nazionali di Frascati (LNF)-INFN, 00044 Frascati, Italy*
(Received 13 December 2006; revised manuscript received 20 April 2007; published 10 September 2007)

This work reports a theoretical study of the x-ray absorption near-edge structure spectra at both the Cu and the Mn *K*-edge in several Cu_2MnM (M=Al, Sn, and In) Heusler alloys. Our results show that *ab initio* single-channel multiple-scattering calculations are able to reproduce the experimental spectra. Moreover, an extensive discussion is presented concerning the role of the final state potential needed to reproduce the experimental data of these half-metallic alloys. In particular, the effects of the cluster size and of the exchange and correlation potential needed in reproducing all the experimental x-ray absorption near edge structure features are discussed.

DOI: 10.1103/PhysRevB.76.104411 PACS number(s): 78.70.Dm, 61.10.Ht

I. INTRODUCTION

X-ray absorption spectroscopy (XAS) constitutes nowadays an outstanding structural tool. The extended x-ray absorption fine structure (EXAFS) part of the spectrum is commonly used to determine the local environment around a selected atomic species in a great variety of systems.[1] Moreover, the near-edge part of the absorption spectrum [x-ray absorption near edge structure (XANES)] becomes an incomparable stereochemical probe because of its high sensitivity to the bonding geometry. This capability is due to the low kinetic energy of the photoelectron that favors the contribution of multiple-scattering processes. For this reason, great effort has been devoted in the last decade to obtain structural determinations from XANES, including bond-angle information. However, the interpretation and the *ab initio* computation of XANES spectra are not so straightforward as for EXAFS.

XANES computation requires sophisticated simulation tools.[2–8] Most of these *ab initio* codes are built within the one-electron multiple-scattering (MS) framework[9] and by using the so-called muffin-tin approximation. More recently, several works appear reporting XANES computations performed within a non-muffin-tin approach[7,10,11] and the promising implementation of the multichannel MS theory.[12,13] Despite the above progresses, the construction of the scattering potential still remains an open problem. Typically, the standard *ab initio* XANES calculations are performed in the framework of the muffin-tin approximation with the addition of an exchange-correlation potential (ECP). In the case of complex ECP potentials, the imaginary part also accounts for the damping of the excited photoelectron. At present, the energy-dependent Hedin-Lundqvist (HL) complex potential[14,15] is the most widely used in *ab initio* XANES calculations.[16] However, it has been reported that in several cases, the energy-dependent Dirac-Hara (DH) exchange potential shows the best agreement to the experimental data,[17–20] although this assignment is not free of controversy.[22–25] As a result, the choice of the ECP among the usual scattering potential set, ranging from real X_α to complex Hedin-Lundqvist, becomes one of the most important steps in obtaining a good reproduction of the experimental spectra. The experience accumulated through the calculation of the absorption cross section for different systems suggests that the HL ECP offers good performance in the case of metals, while for ionic and covalent systems, the use of DH seems to be more adequate.[17–21] However, the variety of reported results indicates that this choice is material specific and, unfortunately, prevents one from *a priori* fixing the ECP for each particular case. In this work, we have faced this problem in connection to the case of half-metallic alloys. These systems present a peculiar behavior associated with the metal and insulator or semiconductor characteristic of the spin subsystems.

The Cu_2MnM (M=Al, Sn, and In) Heusler alloys are interesting magnetic systems because they possess localized magnetic moments although they are all metallic. The magnetic, electrical, and structural properties in these systems are known to be strongly dependent on both the conduction electron concentration and the chemical order.[26–30] Despite the importance of getting a deeper insight in the electronic structure and the chemical bonding mechanism in these compounds, little research has been performed regarding the magnetic polarization of the conduction electrons and its role in the magnetic ordering. Recently, Uemura *et al.* have reported the results of a combined XAS and x-ray magnetic circular dichroism study performed at the *K*-absorption edge of both Mn and Cu in these Cu_2MnM Heusler alloys.[31] Theoretical calculations have been made on the basis of photoelectron full-multiple-scattering theory[32] and by using the Madelung potential taken from the band calculation for Cu_2MnAl performed by Ishida *et al.*[30] According to Uemura *et al.*, the spin-orbit interaction and the exchange scattering are the main factors for the calculation. Thus, even when they used a nonlocal exchange potential that can directly take the spin-polarization effects into account, correlation potential was not included. In addition, only 51 atoms, (5 Å), were included to build up the cluster used for the computations. The fact that computations were performed for such a small cluster and without correlation potential poses serious con-

cerns regarding the reliability of the reached conclusions.

In this work, we present detailed *ab initio* computations of the Mn and Cu *K*-edge XANES spectra in the Cu_2MnM (M=Al, Sn, and In) Heusler alloys. These calculations of the absorption spectra have been made within the multiple-scattering framework. Special attention has been paid to establish the improvements obtained by using different treatments of the exchange-correlation part in the final state potential, intending to obtain the best agreement both in energy and intensity between the experimental and theoretical XANES spectra.

II. COMPUTATIONAL METHODS

The computation of the XANES spectra was carried out using the multiple-scattering code CONTINUUM[4,8] based on the one-electron full-multiple-scattering theory.[9,12] A complete discussion of the procedure can be found in Refs. 15 and 33. Computations were made in parallel mode by using the MPI library.[34]

The potential for the different atomic clusters was approximated by a set of spherically averaged muffin-tin potentials built by following the standard Mattheis' prescription.[35] The muffin-tin radii were determined following the Norman's criterion and by imposing an overlapping factor ranging from 1% to 10%.[36] We have verified that the factor chosen within this range does not affect the spectral shape, and only slight differences are found in the first 5 eV of the computed spectra. After convolution of the spectra to account for both the core-hole lifetime and the experimental resolution, these differences are not significant.

The Coulomb part of each atomic potential was generated using charge densities from the atomic code of nonlocal self-consistent Dirac-Fock code.[5,37] The atomic orbitals were chosen to be neutral for the ground state potential. Two different approximations were tested for the excited state potential: (i) the same potential as for the ground state was used and (ii) relaxed $Z+1$ approximation.[38] During the present calculations, we have found that the screened and relaxed $Z+1$ option leads to the best performance in simulating the experimental absorption spectra at both the Mn and Cu *K*-edges. Finally, we have tested three different choices for the exchange and correlation part of the final state potential: X_α, the energy-dependent HL complex potential, and the energy-dependent DH exchange potential.

The computed spectra have been compared to the experimental XANES data reported by Uemura *et al.*[31] In all the cases, the calculated theoretical spectra have been further convoluted with a Lorentzian shape function $\Gamma=1.5$ eV to account for both the core-hole lifetime[39] and the experimental resolution.

III. RESULTS AND DISCUSSION

Ab initio XANES calculations have been performed at both the Mn and Cu *K*-edges in the case of Cu_2MnAl, Cu_2MnIn, and Cu_2MnSn. These Heusler alloys show the $L2_1$-type (space group $Fm3m$) ordered structure illustrated in Fig. 1. The unit cell contains eight of the small body-centered-cubic cells that can be regarded as four interpenetrating fcc sublattices. There are four kinds of atomic positions: Cu atoms occupy the (1/4,1/4,1/4) and (3/4,3/4,3/4) positions, Mn atoms are at (1/2,1/2,1/2), while the M (Al, In, and Sn) atoms occupy the (0,0,0) position. The lattice parameters are $a=5.957$ Å for Cu_2MnAl;[40] $a=6.166$ Å for Cu_2MnSn,[41] and $a=6.217$ Å for Cu_2MnIn.[42]

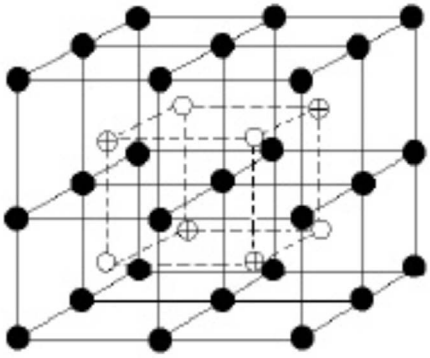

FIG. 1. The stoichiometric Cu_2MnM unit cell: Cu (black circles), Mn (crossed circles), and M (open circles).

The first step of the calculations was made to determine the size of the cluster needed to reproduce all the spectral structures present in the experimental XANES spectra. To this end, we have performed the computation of the Mn *K*-edge XANES in the case of Cu_2MnAl by increasing progressively the number of atoms in the built-up cluster. In this way, we have computed the Mn *K*-edge absorption for clusters containing 59 atoms, i.e., including contributions from neighboring atoms located within the first 5.2 Å around photoabsorbing Mn, 65 (6 Å), 113 (6.7 Å), and 137 (7.3 Å) atoms. The computations, shown in Fig. 2, have been performed by using the real part of the HL ECP and with $l_{max}=4$. The computed spectra show the dependence of both the energy position and the relative intensity of the spectral features as the size of the cluster increases. In the case of the

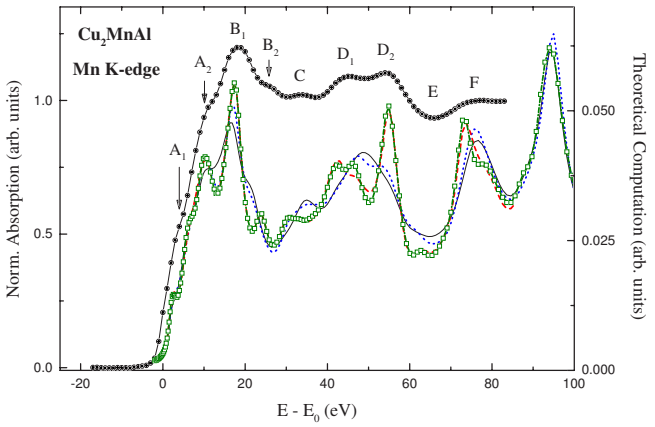

FIG. 2. (Color online) Comparison between the experimental Mn *K*-edge of Cu_2MnAl (•) and the MS computations performed for different cluster sizes covering up to 7.3 Å around the absorbing Mn: 59 (black, solid line), 65 (blue, dotted line), 113 (red, dashed line), and 137 atoms (green, ○).

smallest clusters, 59 and 65 atoms, several spectral features are not reproduced by the calculation. In particular, the B_2 peak ($E \sim 26$ eV), located at the high-energy side of the main B_1 peak is not reproduced. Moreover, for these clusters, the computation yields a broad resonance at ~50 eV, while the experimental spectrum exhibits two well defined peaks D_1 and D_2. In contrast, the computations performed for bigger clusters, 113 and 137 atoms, account for the previously missed structures. In addition, no differences are found within the first 60 eV of the absorption spectrum between the computations performed for clusters including contributions from atoms located within the first 6.7 and 7.3 Å around the photoabsorber. This result indicates that the addition of further coordination shells does not contribute significantly to the XANES spectrum. Accordingly, all the calculations reported henceforth have been obtained by using 169 atoms to generate the scattering potential, but only the scattering contributions of the first 137 atoms (~6.7 Å) are computed.

Next, we have investigated the maximum angular momentum quantum number l_{max} needed to account for the experimental spectrum in the first 100 eV of the absorption spectrum. The choice of $l_{max}=3$ and 4 does not affect the result of the computations in the first 30 eV of the spectrum above the edge. However, for higher energies, both the energy position and intensity of the computed features clearly differ. By increasing l_{max} from 4 to 5, the computed spectra do not change in the simulated spectra in the energy interval of interest, up to $\simeq$80 eV above the edge. Therefore, we have fixed $l_{max}=4$ for all the calculations.

Based on the above results, we have fixed both the cluster size and l_{max}. Then, we have investigated the role of the different ECPs to correctly reproduce the experimental spectra. We have computed the Mn *K*-edge XANES of Cu_2MnAl by using the X_α and the energy-dependent HL and DH ECP potentials.[15] The HL is a complex potential in which its imaginary part accounts for the inelastic losses of the photoelectron. Therefore, we have also made computations by using only the real part of the HL ECP (hereafter, real HL), and, in addition, we have built a "complex" DH one by adding to it the imaginary part of the HL one. The results of the computations are shown in Fig. 3. For the sake of clarity, the comparison between the theoretical spectra and the experimental one has been divided into two panels: (a) one for the real potentials and (b) the second for the complex ones. In the case of the real potentials, the intensity of the spectral features is not in agreement with that experimentally observed as expected, because the photoelectron damping is not taken into account. However, its inspection is rather useful as it allows one to determine that the computations reproduce all the spectral features shown by the experimental spectrum. In this respect, the agreement between the computations and the experimental signal is noticeable as the calculations reproduce the complex profile at the threshold (A_1 and A_2 features), the main peaks (B_1, D_1, D_2, and F), and the two tiny structures (B_2 and C). The performance of the different potentials is similar, although in the case of both X_α and the real HL, the calculated absorption maxima fall short of the observed ones. The addition of the imaginary part of the HL potential improves the calculations. Good agreement between the computations and the experimental

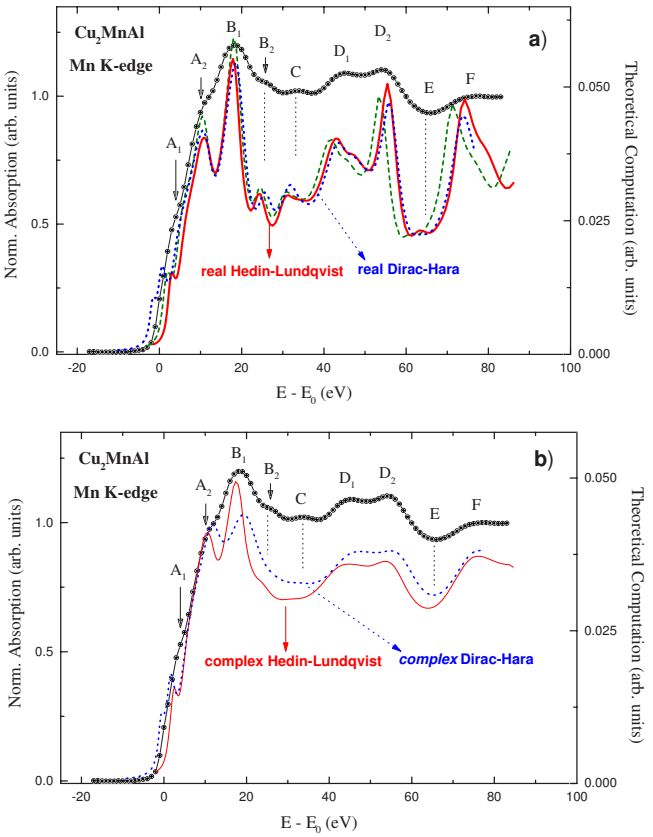

FIG. 3. (Color online) Comparison between the experimental Mn *K*-edge of Cu_2MnAl (○) and the MS computations performed for different ECP potentials: (a) X_α (green, dashed line), real HL (red, solid line), and real DH (blue, dotted line); (b) complex HL (red, solid line) and complex DH (blue, dotted line) (see text for details).

spectrum is obtained for both complex Hedin-Lundqvist ECP by adding to the DH exchange the imaginary part of the HL (hereafter, complex Dirac-Hara). As shown in Fig. 3(b), all the experimental features are properly accounted for by the computations. Complex HL computation yields a better reproduction of the intensity ratio among the different spectral features, specially regarding the main peak B_1 and both A_1 and B_2 features. In contrast, complex DH shows a better reproduction of the relative energy position among the peaks. The experimental energy separation between the main absorption peak B_1 and the negative deep E is $\Delta E=48$ eV, while computation yields 47.6 and 46.2 eV for complex DH and HL, respectively.

We have performed the same class of computations for both Cu_2MnIn and Cu_2MnSn systems. In all cases, we have used $l_{max}=4$ and the potential was created by using a 169 atoms cluster to calculate the scattering contributions of the first 137 atoms. In this way, we account for the contributions from atoms located within the first 6.9 and 6.95 Å around Mn for Cu_2MnSn and Cu_2MnIn, respectively. As shown in Fig. 4, good agreement between the *ab initio* calculations and the experimental data is also found for these compounds. Similarly to the Cu_2MnAl case, the use of the complex DH potential shows better performance than that of the complex HL one in reproducing the energy difference ΔE among the

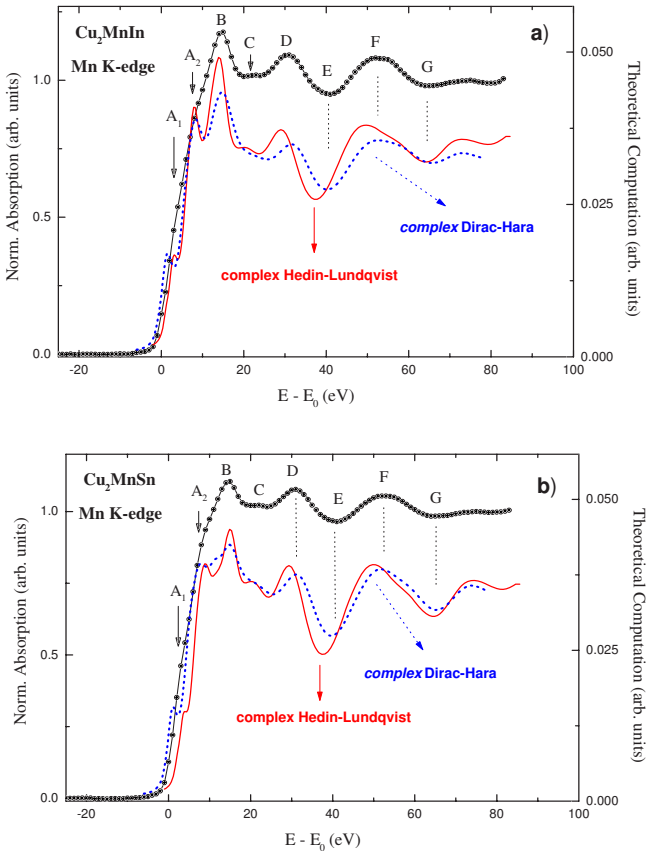

FIG. 4. (Color online) Comparison between the MS computations performed by using both complex HL (red, solid line) and complex DH (blue, dotted line) and the experimental Mn *K*-edge (○) of (a) Cu_2MnIn and (b) Cu_2MnSn.

spectral features. Experimentally, the energy difference between the main peak (B) and the first negative deep (E) is 26 eV for both Cu_2MnIn and Cu_2MnSn compounds. HL computations yield $\Delta E = 23.3$ and 22.5 eV for the In and Sn compounds, respectively. These results are improved by using the complex DH ECP, yielding $\Delta E = 25.9$ and 24.8 eV for Cu_2MnIn and Cu_2MnSn, respectively. As observed for Cu_2MnAl, the intensity ratio of the different spectral features in the first 25 eV of the spectrum is better reproduced by using HL rather than DH ECP. Indeed, the weak structure (C) at the high-energy side of the main peak (B) is correctly reproduced by the HL computation. In contrast, the absorption maxima calculated by using the HL ECP fall short the experimental ones, specially regarding the energy region between 30 and 70 eV above the edge (D–G structures, Fig. 4).

We have extended our study to the Cu *K*-edge in the same materials by following a procedure identical to the one for the Mn *K*-edge. Also in this case, we have verified the need to use $l_{max}=4$ as well as big clusters to reproduce the Cu *K*-edge experimental spectra. Best agreement between the experimental data and the calculations has been obtained by using 169 atoms to generate the potential and by taking into account the scattering contributions of the first 137 atoms. Therefore, contributions from atoms located within the first 6.7, 6.9, and 6.95 Å around Cu are taken into account for Cu_2MnAl, Cu_2MnSn, and Cu_2MnIn, respectively.

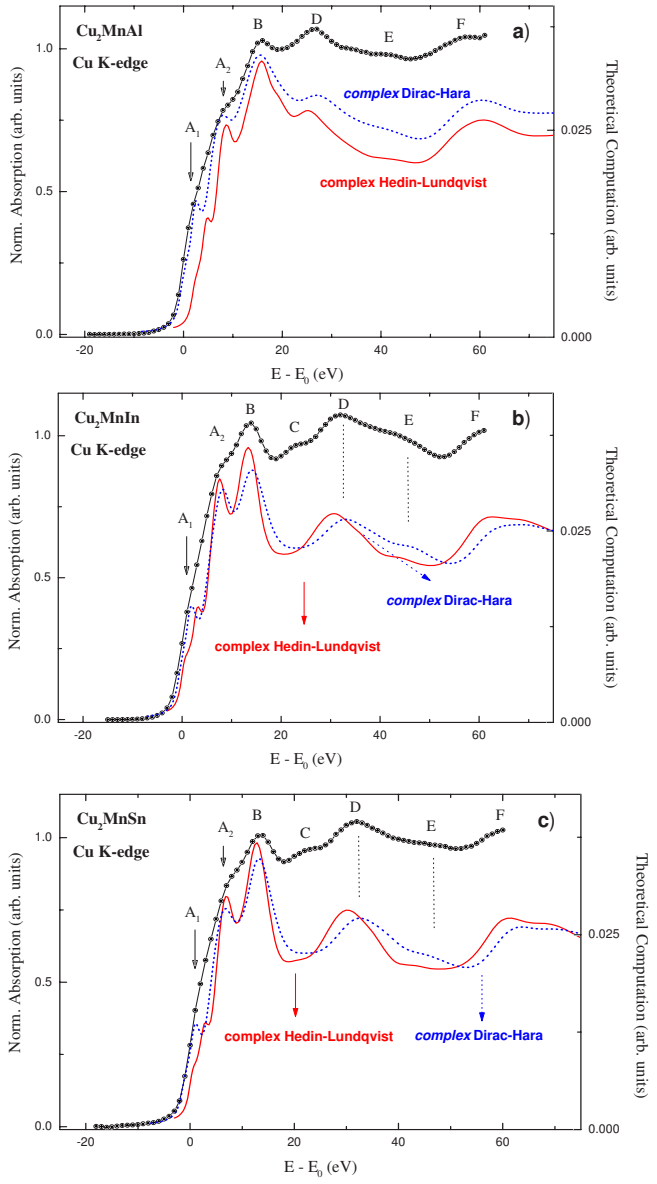

FIG. 5. (Color online) Comparison between the experimental (○) Cu *K*-edge of (a) Cu_2MnAl, (b) Cu_2MnIn, and (c) Cu_2MnSn, and the result of the MS computations performed for both complex HL (red, solid line) and complex DH (blue, dotted line) ECP potentials.

The experimental Cu *K*-edge XANES spectra are similar in the three cases. There are two contributions at the threshold (A_1 and A_2) followed by a prominent peak (B) at ~15 eV in the three compounds. In the case of Cu_2MnAl, there is a single broad resonance (D) at about 27 eV above the edge. In contrast, the spectral profile in this region is different for both Cu_2MnSn and Cu_2MnIn compounds. The Cu *K*-edge XANES of these compounds shows a small structure (C) on the low-energy side of the broad one (D). The emerging feature is located at ~23 eV, while the broad D one is shifted to higher energies (~32 eV) with respect to the Cu_2MnAl case. The theoretical calculations are able to reproduce this trend. As shown in Fig. 5, the computed spectra for both Cu_2MnSn and Cu_2MnIn clearly differ from that

obtained for Cu_2MnAl in the energy region corresponding to C and D features, i.e., from 20 to 35 eV above the edge. The best reproduction of the Cu *K*-edge experimental spectra is obtained by using the complex DH potential. Contrary to the Mn *K*-edge, the improvement of the complex DH ECP over the HL one concerns both the intensity ratio and the relative energy separation between the different spectral features. Indeed, by using the complex HL ECP, the relative intensity of the main contributions to the absorption main peak is not satisfactory and the contraction of the energy scale still persists.

The fact that the agreement between the theoretical calculations and the experiment is better when using the complex DH instead of HL potential is noticeable. Indeed, it is commonly assumed that the HL potential, with its energy-dependent exchange and its imaginary part, is able to reproduce rather accurately the experimental spectra in the case of metals. In contrast, several works have reported the improved performance of the DH potential in accounting for the experimental spectra of ionic systems, insulators, and transition metal oxides.[17–19,24] This result suggests that the treatment of the Coulomb hole correlation by using a single plasmon pole within the *GW* approximation[43] is rather crude in the high-energy region. HL potential is separated into three parts,

$$V^{HL} = V_{ex}^{DH} + V_{sex} + V_{ch}, \tag{1}$$

where V_{ex}^{DH} is the bare exchange Dirac-Hara potential, V_{sex} is the screening of exchange potential, and V_{ch} is the Coulomb correlation hole.[14,15] V_{ex}^{DH} is negative and at high energy asymptotically behaves like k^{-2}. According to several authors, this energy dependence is crucial in the high-energy part of the absorption spectrum, EXAFS.[44,45] V_{sex} is positive, and roughly constant and then rapidly decreases like k^{-4}, while V_{ch}, which describes the repulsion of electrons of the same spin, is negative and its behavior is k^{-1} at high energy.[15] As discussed in Ref. 43, Coulomb correlation hole will lower the energy of the states and, as a consequence, the position of the peaks in continuum state is lowered. The Coulomb correlation hole effect dominates in the higher-energy region, in agreement with our results. Indeed, the comparison of the computations performed by using DH and HL ECP shows that in the latter case, all the peaks in the high-energy region are shifted to a lower-energy position. This result reflects the inadequacy of using a single plasmon pole within the *GW* approximation[43] to account for the Coulomb hole correlation in the high-energy region.

IV. SUMMARY AND CONCLUSIONS

We have presented the detailed *ab initio* computation of the Mn and Cu *K*-edge XANES spectra in the case of Cu_2MnM (M=Al, Sn, and In) compounds performed within the multiple-scattering framework.

The comparison between the experimental data at the two edges and the theoretical calculations has demonstrated the need to use large clusters, ~7 Å around central photoabsorbing atom, either Mn or Cu, to reproduce the experimental spectra of these Heusler alloys.

During the multiple-scattering *ab initio* calculations, we have tested different exchange and correlation possibilities to construct the final state potentials. Contrary to the current expectation for metallic systems of obtaining the best reproduction of the experimental XANES spectra by using the Hedin-Lundqvist potential, the best agreement is obtained, specially in the Cu *K*-edge case, by using the Dirac-Hara ECP.

We concluded that Hedin-Lundqvist potential overestimates the effect of the Coulomb correlation hole in the high-energy region, resulting in an unphysical contraction of the computed spectra by lowering in energy the calculated peak positions. This problem is solved by adding to the real energy-dependent Dirac-Hara potential and the imaginary part of the Hedin-Lundqvist ECP. In this way, the inelastic losses of the photoelectron are accounted for and both the relative energy position and the intensity ratio among the different spectral features are properly accounted for by the computations.

ACKNOWLEDGMENTS

This work was partially supported by the Spanish CICYT (Grant No. MAT2005-06806-C04-04). K.H. acknowledges a grant from Aragón DGA (research mobility program), and J.C. acknowledges the Japanese Society for the Promotion of Science, Japan. We acknowledge H. Maruyama for providing us the experimental spectra.

*Present address: Università degli studi Roma Tre, Dipartimento di Fisica, Via Vasca Navale 84, Rome, I-00146 Italy.

[1] For a review see, for example, in *X-Ray Absorption: Principles, Applications, Techniques of EXAFS, SEXAFS, XANES*, edited by R. Prins and D. Koningsberger (Wiley, New York, 1988), and references therein.

[2] P. J. Durham, J. B. Pendry, and C. H. Hodges, Comput. Phys. Commun. **25**, 193 (1982).

[3] D. D. Vvedensky, D. K. Saldin, and J. B. Pendry, Comput. Phys. Commun. **40**, 421 (1986).

[4] C. R. Natoli and M. Benfatto (unpublished); M. Benfatto, C. R. Natoli, A. Bianconi, J. García, A. Marcelli, M. Fanfoni, and I. Davoli, Phys. Rev. B **34**, 5774 (1986).

[5] A. L. Ankudinov, B. Ravel, J. J. Rehr, and S. D. Conradson, Phys. Rev. B **58**, 7565 (1998).

[6] A. Filipponi, A. Di Cicco, T. A. Tyson, and C. R. Natoli, Solid State Commun. **78**, 265 (1991); A. Filipponi, A. Di Cicco, and C. R. Natoli, Phys. Rev. B **52**, 15122 (1995); A. Filipponi and A. Di Cicco, TASK Q. **4**, 575 (2000).

[7] Y. Joly, D. Cabaret, H. Renevier, and C. R. Natoli, Phys. Rev. Lett. **82**, 2398 (1999).

[8] M. Benfatto and S. Della Longa, J. Synchrotron Radiat. **8**, 1087

(2001); S. Della Longa, A. Arcovito, M. Girasole, J. L. Hazemann, and M. Benfatto, Phys. Rev. Lett. **87**, 155501 (2001).
[9] P. A. Lee and J. B. Pendry, Phys. Rev. B **11**, 2795 (1975).
[10] Y. Joly, Phys. Rev. B **63**, 125120 (2001).
[11] K. Hatada, K. Hayakawa, M. Benfatto, and C. R. Natoli, Phys. Rev. B **76**, 060102(R) (2007).
[12] C. R. Natoli, M. Benfatto, C. Brouder, M. F. Ruiz Lopez, and D. L. Foulis, Phys. Rev. B **42**, 1944 (1990).
[13] P. Krüger and C. R. Natoli, Phys. Rev. B **70**, 245120 (2004).
[14] L. Hedin and B. I. Lundqvist, J. Phys. C **4**, 2064 (1971).
[15] C. R. Natoli, M. Benfatto, S. Della Longa, and K. Hatada, J. Synchrotron Radiat. **10**, 26 (2003).
[16] J. J. Rehr and R. C. Albers, Rev. Mod. Phys. **72**, 621 (2000).
[17] R. Gunnella, M. Benfatto, A. Marcelli, and C. R. Natoli, Solid State Commun. **76**, 109 (1990).
[18] S. Díaz-Moreno, A. Muñoz-Páez, and J. Chaboy, J. Phys. Chem. A **104**, 1278 (2000).
[19] M. F. Ruiz-Lopez and A. Muñoz-Paez, J. Phys.: Condens. Matter **3**, 8981 (1991).
[20] V. Briois, Ph. Sainctavit, and A.-M. Flank, Jpn. J. Appl. Phys., Suppl. **32**, 52 (1993).
[21] H. Modrow, S. Bucher, J. J. Rehr, and A. L. Ankudinov, Phys. Rev. B **67**, 035123 (2003).
[22] J. Chaboy, M. Benfatto, and I. Davoli, Phys. Rev. B **52**, 10014 (1995).
[23] V. Jeanne-Rose and B. Poumellec, J. Phys.: Condens. Matter **11**, 1123 (1999).
[24] D. Cabaret, Ph. Sainctavit, Ph. Ildefonse, and A.-M. Flank, J. Phys.: Condens. Matter **8**, 3691 (1996).
[25] D. Cabaret, M. Le-Grand, A. Ramos, A.-M. Flank, S. Rossano, L. Galoisy, G. Calas, and D. Ghaleb, J. Non-Cryst. Solids **289**, 1 (2001).
[26] P. J. Webster and R. S. Tebble, Philos. Mag. **16**, 337 (1976).
[27] P. J. Webster and M. R. I. Ramadan, J. Magn. Magn. Mater. **13**, 301 (1979).
[28] D. P. Oxley, R. S. Tebble, and K. C. Williams, J. Appl. Phys. **34**, 1362 (1963).
[29] J. Soltys, M. Stefaniak, and J. Holender, Philos. Mag. B **49**, 151 (1984).
[30] S. Ishida, J. Ishida, S. Asano, and J. Yamashita, J. Phys. Soc. Jpn. **45**, 1239 (1978).
[31] S. Uemura, H. Maruyama, N. Kawamura, H. Yamazaki, S. Nagamatsu, and T. Fujikawa, J. Synchrotron Radiat. **8**, 452 (2001).
[32] T. Fujikawa, J. Phys. Soc. Jpn. **62**, 2155 (1993).
[33] See, for example, J. Chaboy and S. Quartieri, Phys. Rev. B **52**, 6349 (1995), and references therein.
[34] See, for example, http://www-unix.mcs.anl.gov/mpi/
[35] L. F. Mattheis, Phys. Rev. **133**, A1399 (1964); **134**, A970 (1964).
[36] J. G. Norman, Mol. Phys. **81**, 1191 (1974).
[37] J. P. Desclaux, Comput. Phys. Commun. **9**, 31 (1975).
[38] P. A. Lee and G. Beni, Phys. Rev. B **15**, 2862 (1977).
[39] M. O. Krause and J. H. Oliver, J. Phys. Chem. Ref. Data **8**, 329 (1979).
[40] J. Soltys, Phys. Status Solidi A **66**, 485 (1981).
[41] E. Uhl, J. Magn. Magn. Mater. **25**, 221 (1981).
[42] P. J. Webster, K. R. A. Ziebeck, and R. M. Mankikar, J. Magn. Magn. Mater. **54**, 1355 (1986).
[43] L. Hedin, Phys. Rev. **139**, A796 (1965).
[44] S. H. Chou, F. W. Kutzler, D. E. Ellis, G. K. Shenoy, T. I. Morrison, and P. A. Montano, Phys. Rev. B **31**, 1069 (1985).
[45] S. H. Chou, J. J. Rehr, E. A. Stern, and E. R. Davidson, Phys. Rev. B **35**, 2604 (1987).